Electrochemical Preparation and Characterization of Surface-Fluorinated TiO_2 Nanoporous Film and Its Enhanced Photoelectrochemical and Photocatalytic Properties

X. F. Cheng,[†] W. H. Leng,*[,†] D. P. Liu,[†] Y. M. Xu,[†] J. Q. Zhang,[†] and C. N. Cao[†,‡]

Department of Chemistry, Yuquan Campus, Zhejiang University, Hangzhou, 310027, China, and State Key Laboratory for Corrosion and Protection of Metals, Institute of Metal Research, Chinese Academy of Sciences, Shenyang 110016, China

Received: October 5, 2007; Revised Manuscript Received: March 1, 2008

In recent years, surface fluorination of TiO_2 has been demonstrated to be an efficient method for improving its photocatalytic (PC) reactivity toward some pollutants. In this paper, a new and simple method for surface fluorination and porosity-creating of TiO_2 is presented. The sample was prepared by anodization of TiO_2 in HF aqueous solutions formed by direct thermal oxidization of titanium sheet. The preparation conditions were optimized. The prepared samples were characterized by scanning electron microscopy (SEM), Raman spectroscopy, UV–vis diffuse reflectance spectroscopy (DRS), X-ray photoelectron spectroscopy (XPS), and photoluminescence (PL). The photoelectrochemical (PEC) and photocatalytic (PC) properties of the samples were also investigated. SEM and Raman showed that the anodization made the TiO_2 nanoporous, which consequently increased markedly the specific surface area, but did not change the bulk crystal structure under a certain preparation condition. DRS analysis revealed that the light absorption was decreased after electrochemical etching. The band gap energy narrowed from 3.15 to 3.04 eV. The surface fluorination of the etched-TiO_2 was evidently supported by XPS. Highly enhanced PEC performance and PC activities for the degradation of target pollutants, phenol, methylene blue, and reactive brilliant red on the etched-TiO_2 were observed. The possible reasons for such an improvement were studied in detail by a combination of the above-mentioned methods and (photo) electrochemical techniques. It is mainly attributed to the enhanced specific surface area, negative-shifted appearing energy band edges, decreased surface recombination centers, and/or favorable charge transfer rate. The F-containing TiO_2 electrode has an excellent stability against fluoride desorption.

1. Introduction

Semiconductor photocatalysis has been intensively investigated for potential application in environmental pollutant degradation, water splitting, and photoelectric conversion.[1–5] Among various semiconductors, TiO_2 has been mostly studied, due to its high performance in photocatalytic (PC) activity and chemical stability and low cost in production and friendliness to the environment.[2–5] However, the quantum yield of the TiO_2-based reaction achieved so far is still very low (typically less than 0.1).[2] Therefore, further improvement of TiO_2 photoactivity is undoubtedly needed.

Because PC reactions primarily take place on the catalyst surface, the reaction efficiencies and related mechanisms would be greatly determined by surface properties, such as surface area, surface acidity, surface defects, surface complexes, particle size, crystalline phase, and so on.[6,7] Recently, surface modification of TiO_2 with fluoride anions has widely been investigated.[6–18] It has been shown that the fluorinated TiO_2 (F-TiO_2) can result in great improvement in the oxidation rate of phenol,[6,7] benzene,[8] reactive brilliant red (X3B),[9] and so on. There are only a few negative results, that the reaction rate was decreased upon surface fluorination, for instance, in the dechlorination of trichloroacetic acid.[7] The relevant mechanism involving surface fluorination and PC reactions has been discussed,[6,7] but it still remains unclear to some extent.[10,11] The majority view is that an enhanced *free* OH radicals is produced due to the fluoride replacement of surface hydroxyl groups.[7–9] However, the physical chemistry nature thereof is not clear yet. On the other hand, direct introduction of fluoride atoms into the TiO_2 lattice (F-doped TiO_2) has also been studied.[12–18] This kind of fluorination can improve the crystallinity of anatase and thus the PC reactivity.[12,13] It also results in fewer anion vacancies and lower density of midgap states, and thus higher stability against photocorrosion as compared to the undoped TiO_2.[13–15] Very recently, a new method of vapor phase fluorination at 473 K using anhydrous hydrogen fluoride has been reported.[16] The as-prepared TiO_2 can facilitate photoevolution of H_2 from water, photodegradation of aldehyde and methylene blue, and photo-induced hydrophilicity under UV light irradiation.[16] However, this method of TiO_2 fluorination has shortcomings of high temperature and complex equipments.

It is well-known that electrochemical etching is a simple and effective means to produce holes at semiconductor[19] and metal.[20–22] For example, Si anodization process, which is electrochemical dissolution of Si in aqueous HF solution, has been developed to achieve formation of high-aspect-ratio pores.[19] Interestingly, it has been mentioned recently that the surface concentration of fluoride on a freshly prepared TiO_2 nanotubes via anodic Ti oxidation in hydrofluoric acid medium can be high as much as 13.7 at.%.[21] Taking into account the above aspects, we expect that such surface fluorination by anodization etching of TiO_2 in aqueous HF solutions may also result in an increase in photoelectrochemical (PEC) and PC performance. To the best of our knowledge, this effect of surface

* To whom correspondence should be addressed. Tel: +86 571 87952318. Fax: +86 571 87951895. E-mail: lengwh@css.zju.edu.cn.
[†] Zhejiang University.
[‡] Chinese Academy of Sciences.

10.1021/jp7097476 CCC: $40.75
Published on Web 05/21/2008

fluorination on the TiO_2 PEC and PC has not been reported in the literature.

This paper addresses the PEC and PC properties of surface fluorinated TiO_2 film, prepared by a simple electrochemical etching method in HF solutions. Phenol and dyes (methylene blue and X3B) were used as the model compounds. The prepared TiO_2 films were characterized by scanning electron microscopy (SEM), Raman spectroscopy, UV–vis diffuse reflectance spectroscopy (DRS), X-ray photoelectron spectroscopy (XPS), photoluminescence (PL), and (photo) electrochemical techniques, respectively. The origin of enhanced PEC and PC activities is discussed in detail.

2. Experimental Section

2.1. Preparation. All chemicals and solvents were of analytical grade and used as received without further purification. Doubly distilled water was used in all experiments. Rutile TiO_2 film was fluorinated unless otherwise stated. Briefly, the film was obtained by direct thermal oxidization of titanium sheet in a furnace under air at 600 °C (denoted as TO-TiO_2).[5] For comparison, anatase TiO_2 film was also studied, which was fabricated by dip-coating of TiO_2 sol onto Ti substrate, followed by heat treatment (total layers were 14).[5]

Electrochemical anodic etching experiment was carried out in a two-electrode system with Pt plate as counter electrode and the TiO_2 film as working electrode. The distance between two electrodes was 2 cm. The electrode was etched in a 0.5 M H_2SO_4 solution containing 0.5% NaF by applying an anodic potential. Maximum photocurrent was obtained at 10 V for 5 min, and thus the electrode etching was mostly conducted under such conditions, except otherwise specified. After etching, the films were thoroughly washed with water and dried in air at room temperature for use. Then the film electrode was weld with nickel wire on the backsides for an electrical contact. The working area of the electrode was 20 and 0.64 cm^2 for PC and PEC/electrochemical measurements, respectively, and the rest of the electrode was covered with epoxy.

2.2. Characterization. The film morphologies were characterized using SEM (FEI Sirion-200, Holland) operated at an accelerating voltage of 20 kV. XPS (VG ESCALAB MK-II, U.S.A.) was performed with Mg Kα radiation at 50 eV. The binding energy was referenced to the C1s level (284.5 eV) due to surface contaminants. Raman spectra were measured on an Almega laser Raman spectrometer (Thermo Nicolet, U.S.A.). DRS were recorded on a UV-2401 PC spectrometer with a labsphere diffuse reflectance accessory using $BaSO_4$ as the background. The PL study of the film was carried out using a Hitachi 850 spectrophotometer with a He−Cd laser as excitation source. The film thickness (mg cm^{-2}) was measured by a gravimetric method.

2.3. PEC and Electrochemical Measurements. All measurements were carried out in a conventional three-electrode cell with a quartz window, using a saturated calomel electrode (SCE) as reference electrode and a platinum wire as counter electrode. The electrolyte was 0.5 M Na_2SO_4, and the solution pH was adjusted with H_2SO_4 and/or NaOH. During the photocurrent measurements, oxygen-free nitrogen at a rate of 16 cm^3 h^{-1} through pipettes with porosity glass frit was bubbled for removal of oxygen from the anode compartment. The potential for both current–potential and impedance measurements was controlled by a model EG&G 273A potentiostat (Princeton Applied Research) coupled to a lock-in amplifier (EG&G M5210).

For most experiments, the light source was a 500 W Xe lamp, and a water filter made from a Pyrex glass was used to minimize heating and to remove UV light at $\lambda < 300$ nm. The average intensity of incident light was 3.0 mW cm^{-2}, measured by a UV-irradiance meter (UV-A, Instruments of Beijing Normal University, China). The incident photon to current efficiency (IPCE) was measured using a 250 W xenon lamp (SVX 1450, Müller Germany) equipped with a monochromator (Acton Spectra Pro-150, U.S.A.) that was used as light source.[23,24] The photon density of monochromatic light was monitored by an irradiatometer (S370, UDT Instruments, and U.S.A.).

The differential capacitance versus voltage was acquired by an impedance method. By stepping the potential from positive to negative potential, the impedance response was measured at each potential. The magnitude amplitude of the ac modulation was set at 10 mV and 3 mV for evaluating flatband potential (E_{fb}) and analyzing surface states, respectively.

2.4. Photoactivity Measurement. Experiments for both PC and electro-assisted PC degradation of the target pollutants were performed in a single-compartment rectangular Teflon cell (solutions 50 cm^3). The TiO_2 film electrode was used as a working electrode, a large area Pt plate as a counter electrode, and SCE as a reference electrode, respectively. The initial concentration of target pollutant was 10 mg dm^{-3}. Prior to illumination, the solution was bubbled with air for 15 min so as to achieve adsorption equilibrium. Then the solution was stirred under O_2 bubbling throughout the experiments, and irradiated with a 300 W Hg lamp. The incident light intensity into the reactor was measured to be 15.2 mW cm^{-2}. Substrate concentration was spectrophotometrically analyzed on a UV-2500 spectrometer (Shimadzu, Japan). The detected wavelength was 510 nm for phenol via 4-aminoantipyrine colorimetric method,[25] 656 nm for methylene blue, and 520 nm for X3B.[9,26]

3. Results

3.1. Effect of Etching Potential and Time on the PEC Performance. In general terms, the efficiency of PC process is determined by the generation, recombination and transfer to the solution of charge carriers (electrons/holes).[1,6] If the overall interfacial electron transfer rate (difference in rate between hole and electron transfer) or photocurrent is large, we say that the PEC performance is high and favors the occurrence of the chemical reaction. The PC activity of photocatalyst is usually described in term of the photooxidation rate of pollutant which is not only dependent on the number of holes available but also on the concentration of pollutant on the surface. Note that large photocurrent does not necessarily correspond to high PC activity since a part of the photocurrent may be used for water oxidation rather than for pollutant oxidation.[5]

First, the effect of etching conditions on the electrode PEC performance was studied. The performance of the films was evaluated in terms of the photocurrent at 0.8 V in 0.5 M Na_2SO_4 (pH 3) which was defined as the difference between the currents under illumination and in the dark. The results are listed in Table 1. Obviously, the photocurrent is strongly dependent on the etched potential and time. The highest photocurrent appeared at 10 V for 5 min. When the TiO_2 electrode was dipped in HF solution without applying a potential or in a fluoride-free solution with exerting a potential, no obvious improvement in the photocurrent was observed. These results indicate that the enhanced PEC performance is due to the coeffect of electric filed and F^- ions. Thus, all the etched-TiO_2 electrodes used for the following study were only prepared under such an optimized conditions (10 V and 5 min), unless specified otherwise. It is worth mentioning that the enhanced PEC performance was also observed with the anatase TiO_2 electrodes upon this treatment (Figure S1, Supporting Information).

TABLE 1: Effect of Etching Potential and Time on the Photocurrent of TiO_2 Electrode in 0.5 M Na_2SO_4 at pH 3

etching potential/V	etching time/min	photocurrent density/μA cm^{-2}
0	5	78
2	5	80
5	5	114
10	5	213
20	5	20
30	5	8
10	2	98
10[a]	5	69
10	10	46
10	30	9
0[b]	0	81

[a] Treated in 0.5 M H_2SO_4 without NaF. [b] TiO_2 unetched.

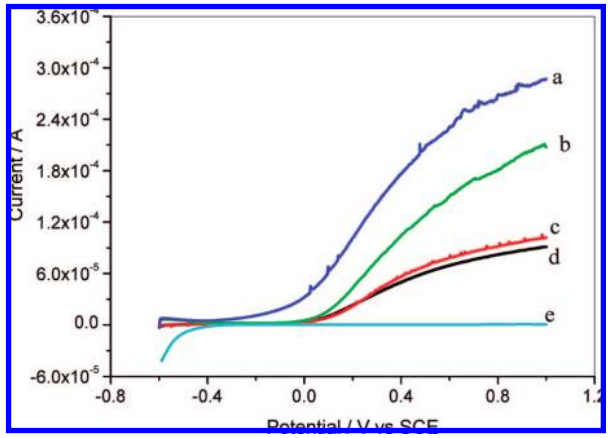

Figure 1. Linear sweep voltammogram under illumination for: (a) etched-TiO_2 + 0.1 M formate; (b) etched-TiO_2 + blank electrolyte; (c) unetched TiO_2 + blank electrolyte; (d) unetched TiO_2 + 0.1 M formate; (e) etched-TiO_2 in the dark. Scan from −0.6 to +1.0 V at a rate 50 mV s^{-1}. The blank electrolyte is 0.5 M Na_2SO_4 (pH = 3) with the bubble of N_2 during the experiment.

Second, the potential dependence of photocurrent for the etched and unetched electrodes in blank solutions or in 0.1 M formate (pH 3) was studied. The results are shown in Figure 1. The photocurrent of the etched-TiO_2 either in Na_2SO_4 or in formate (curves a and b) was greatly improved in the whole positive potential range, as compared to that of untreated TiO_2 (curves c and d). A similar phenomenon was also observed in pH 11 solutions (results not shown). This further indicates that some changes have been made by the etching process. Interestingly, the etched electrode is more sensitive to formate than the untreated TiO_2 in the potential dependence of photocurrent. Similar result of methanol as formate was also observed with this kind of rutile TiO_2 electrode (result not shown).

Third, the photocurrent action spectrum was also measured for the two electrodes. The results are shown in Figure 2. The etched TiO_2 displays a higher value of IPCE than the unetched TiO_2 in the wavelength region of 300−380 nm. Particularly, the value of IPCE at 330 nm is increased from 40 to 90% upon the etching process.

3.2. Morphology, Size, Crystal Structure, and Film Thickness. Figure 3 shows typical SEM micrographs for the unetched and etched TiO_2 electrodes. The former is uniform, only with some grains and grain boundaries on the surface, but without grooves or pores. However, after etching, the surface morphology changed dramatically. A highly porous network with structural details in 50–200 nm can be observed. Further magnification of the graph (Figure 3, B2 and B3) shows that

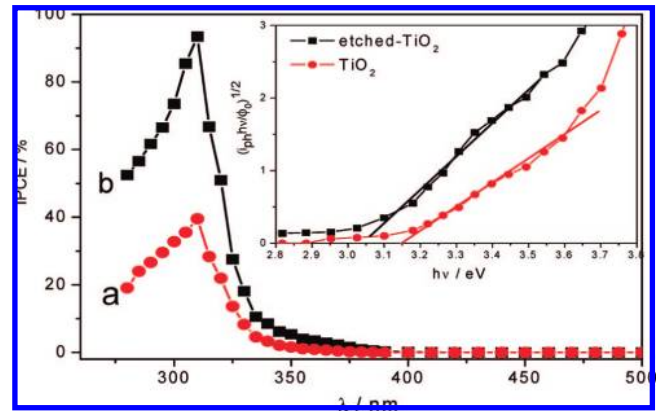

Figure 2. IPCE at 0.8 V in 0.5 M Na_2SO_4 (pH 3) as a function of wavelength (λ). (a) Unetched TiO_2 electrode, and (b) TiO_2 electrode etched at +10 V for 5 min in the dark. (inset) Plot of $(i_{ph}\,h\nu/\Phi_0)^{1/2}$ versus photon energy ($h\nu$) for the two electrodes used for estimation of the band gap energy; where i_{ph} is the photocurrent and Φ_0 is the incident light intensity; for more details, see the text.

there are nanocrystalline (about 20–50 nm) on the inner wall of these grooves and pits on the raised nanocells. Such structural change would result in an increased surface area, beneficial to the PC reactions on the catalyst surface.

The crystal form of the TiO_2 films did not change upon etching, and both the films were in the form of rutile as revealed by Raman spectra and X-ray diffraction (XRD) (Figure S2, Supporting Information).

The film thickness (mg cm^{-2}) of the electrodes was calculated from the mass changes of a larger area of titanium sheet (6 cm × 10 cm) thermally oxidized at the same conditions as the smaller. The film thickness of the resultant pure TiO_2 electrodes was 1.25 mg cm^{-2}, or estimated to be 3.0 μm using the bulk density of rutile ρ = 4.0 g cm^{-3} assuming that the film is compact. After etching, its mass decreased and the film thickness reduced to be 0.80 mg cm^{-2}, or 2.0 μm using the same density and not considering the porosity of the film. The fact that an enhanced PEC performance can still be observed though the amount of catalyst was reduced after etching suggests that other factors should contribute to this.

3.3. Chemical States of Fluorine. Figure 4A shows the XPS survey spectra of the unetched and etched-TiO_2 films. Obviously, all elements of Ti, O, and C exist on the surfaces of both electrodes, whereas F is only detected with etched-TiO_2, as expected. On the basis of the area ratios of F 1s to Ti 2p, the atomic ratio of fluorine to titanium was estimated to be 0.07 with etched-TiO_2 electrode. Figure 4B shows the highly resolved XPS spectra of F 1s for the two etched-TiO_2 electrodes, where sample A is freshly etched and sample B is the electrode that has been used for 5 times in the PEC experiments followed by storage in air for 30 days. The main peak 1 at about 686 eV can be assigned to the F species in solid $TiOF_2$ phase,[17] probably due to nucleophilic substitution of F^- ions during the etching process. The peak 2 at 688 eV is very close to that reported by Yu et al. ascribed to the substitutional fluorine in the crystal lattice of TiO_2.[13] The peak at 684 eV assigned to F^- ions adsorbed on the TiO_2 surface[7] was not observed due to washing with water. The XPS spectra of F 1s for the two etched electrodes are almost the same, indicating that this kind of fluorination is quite stable. So herein the added fluorine mainly exists in the form of $TiOF_2$, rather than that physically adsorbed on the surface. Such $TiOF_2$ phase was not observed in the Raman pattern, possibly due to its low concentration.

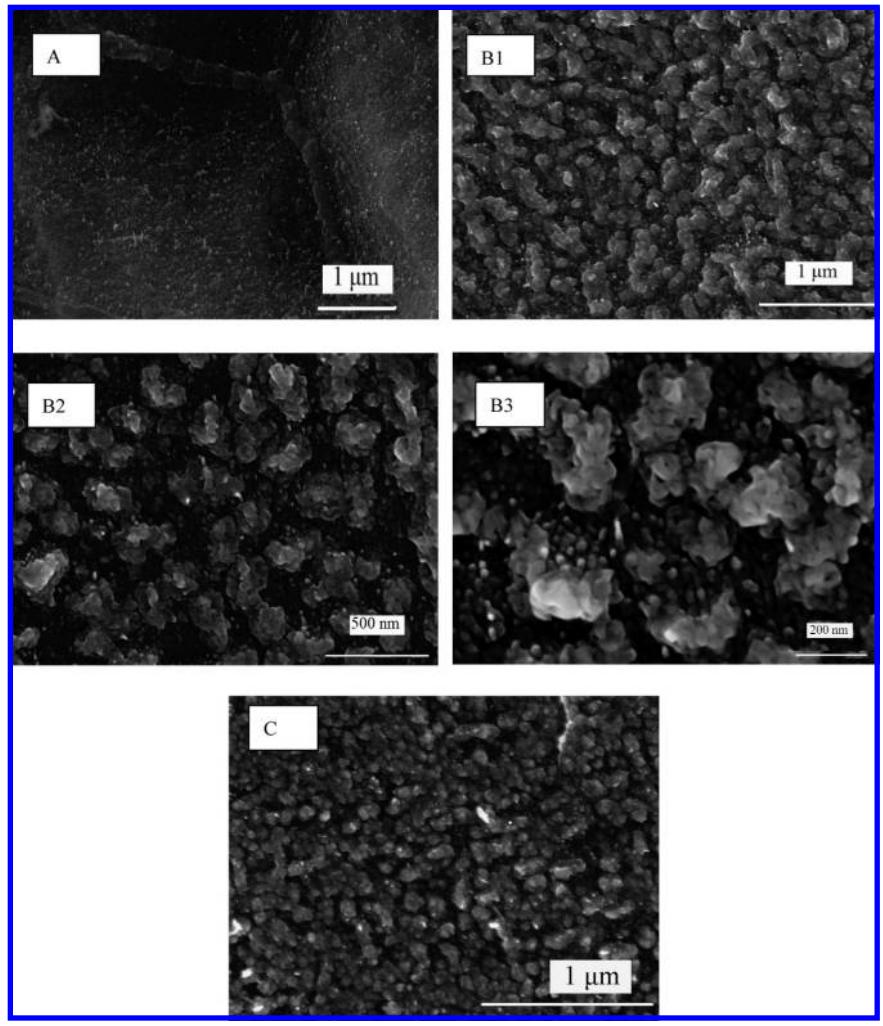

Figure 3. Typical SEM images of TiO_2 film electrodes. (A) Without anodic etching. (B) Etching at +10 V for 5 min in HF solutions. Surface of the etched-TiO_2 is shown at three levels of magnification as shown in B1, B2, and B3. (C) Same as B but after heating at 400 °C in air.

3.4. Photoabsorbance Property. Figure 5 shows the UV–vis DRS spectrum of the two film electrodes. Significant absorption at wavelength shorter than 400 nm can be assign to the interband transition from occupied O 2p orbital to empty Ti 3d orbital of pure rutile TiO_2 (3.0 eV).[4] The etched-TiO_2 shows a weaker absorption than the unetched. This contrasts with the higher absorbance obtained with the F-doped TiO_2[13] and F-adsorbed TiO_2.[7] This may be contributed to the film thinning due to etching. It is worthy to note that at wavelengths longer than 410 nm below its absorption edge, the unetched TiO_2 exhibits a weak and broadened absorption band, as compared to the etched TiO_2. This can be assigned to the midgap levels in TiO_2. In this regard, the disappearance of such broadened band in the etched-TiO_2 might suggest that the density of surface states is reduced upon etching process, which will be further discussed below.

3.5. PL Spectra. This technique has been widely used in the PEC field over solid semiconductors as a useful probe for understanding the surface process in which photogenerated electrons and holes take part.[25,27] Figure 6 shows the PL emission spectra of the etched-TiO_2 along with the pure TiO_2. The emission spectra shapes are similar and a series of peaks are presented for the two electrodes. As reported, these peaks were formed by the combination of different excitation–emission paths.[18,27] The detailed PL mechanism should be complex and is under the scope of this paper. However, some conclusions can be drawn from the spectra. For instance, the emission band at 390 nm is mainly due to free excitation–emission of TiO_2, whereas the emission band at 442 nm should result from surface states. The peak positions in the PL of the etched-TiO_2 are essentially the same as that of the pure TiO_2, whereas the PL intensities for the former are lower than the latter. Because excitation was carried out under equal absorption conditions at 225 nm, the lower intensity usually represents a lower recombination rate of the photogenerated carriers,[25,27] particularly for the visible luminescence peak at 442 nm of the etched electrode is obviously quenched, which indicates that the etching slowed down the radiative recombination process of photocarriers in the electrode. In other words, the etching decreased the density of the luminescence center/recombination center (surface states). The similar phenomena have been reported for some metal-doped TiO_2.[25]

3.6. Flatband Potential and Energy Band Structure. The flatband potentials of the TiO_2 electrodes can be measured via the Mott–Schottky (M-S) relations when the space charge layer is in depletion.[4,28,29] Figure 7 shows the M-S plots for the etched and unetched TiO_2 electrodes at pH 10. It was found that after etching, the value of E_{fb} shifted negatively from *ca.* −0.58 to −0.72 V at pH 10. The value of E_{fb} for the unetched TiO_2 is in good agreement with that reported by Cooper et al.[28] Wang and Mallouk have reported that specific adsorption of fluoride ions, at millimolar concentration in acetonitrile, leads to a large negative shift of E_{fb}.[14] Similar negative shift upon fluorination is first reported here in aqueous solution. In fact, Figure 1 has

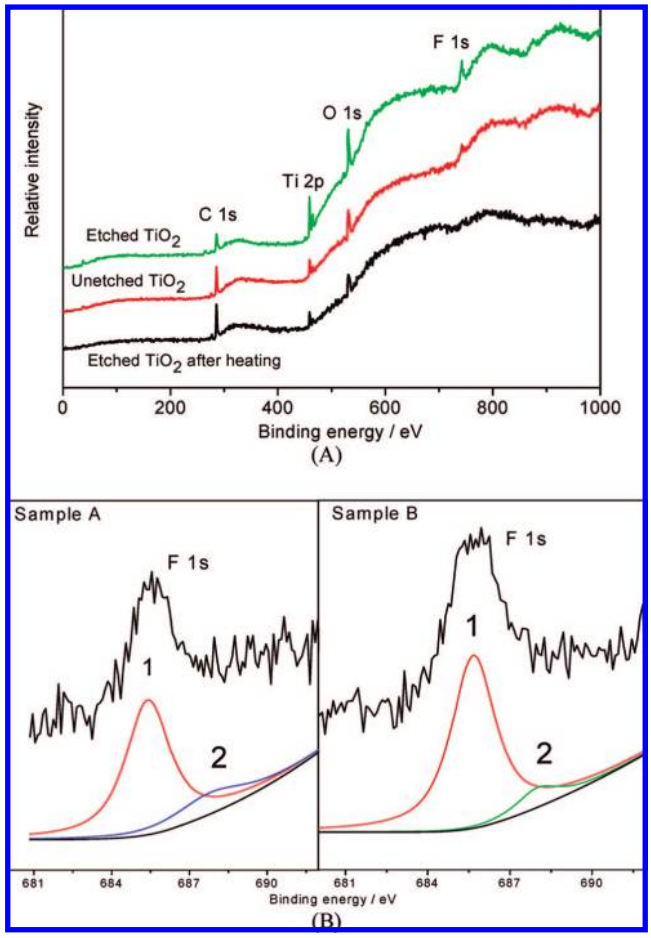

Figure 4. (A) X-ray photoelectron spectra of the unetched electrodes, the etched electrodes, and the etched TiO_2 but after heating at 400 °C in air. (B) F1s high-resolution XPS spectra of two etched-TiO_2: sample A is freshly prepared and sample B is after PEC experiments (see the text for details). XPS peaks after baseline subtraction were resolved into individual components with a nonlinear least-squares procedure.

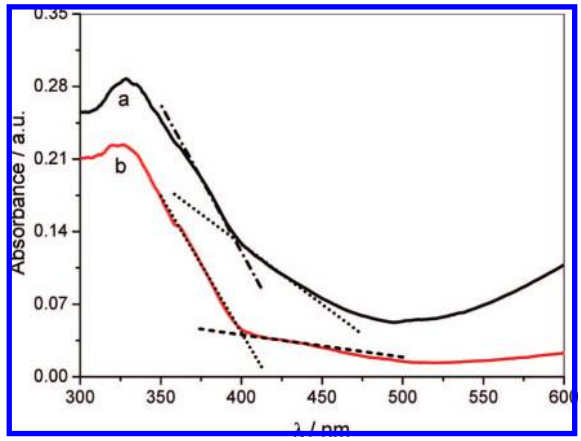

Figure 5. UV–vis diffuse reflectance absorption spectra of (a) TiO_2 without etching and (b) TiO_2 etched at 10 V for 5 min. $BaSO_4$ was used as the reference. The cross point of the two dash tangents is used to estimate the absorption edge of the electrodes. For more details, see the text.

shown an indirect evidence for that. According to the well-known Gärtner equation, where only the recombination of photocarriers in bulk phase is considered,[4] the onset potential of photocurrent corresponds to the flat band potential. The pH dependence of E_{fb} for the two electrodes is also summarized in the inset of Figure 7. The linear plots are in good agreement

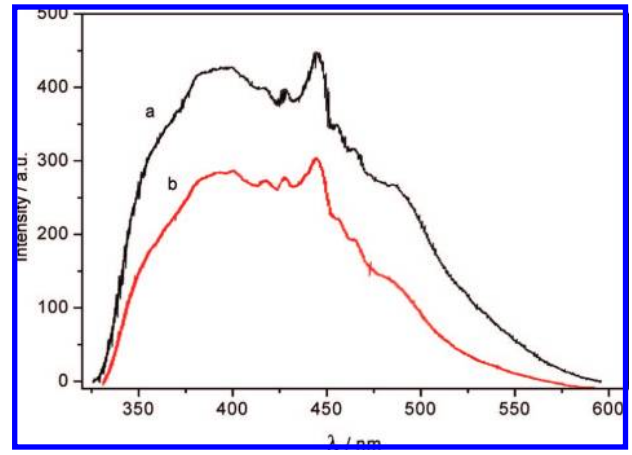

Figure 6. Photoluminescence emission spectra of (a) TiO_2 and (b) the etched-TiO_2 film electrodes. The excitation wavelength was 225 nm.

with the Nernstian equation,[4,29] with a slope of −57 mV and −53 mV/pH unit for the etched and unetched TiO_2 electrodes, respectively. In aqueous solutions, similar shift of E_{fb} with pH has been reported even with surface-fluorinated TiO_2, suggesting that the electrode surface is also covered partially by OH^- groups.

To obtain the band edge potential of the electrode, one needs to know the effective donor density, N_D. It can be calculated from the slope of the linear M−S plot, taking the value of relative dielectric constant of the oxides to be 173.[4] The calculated value is 1.31 and 3.26×10^{19} cm^{-3} for the unetched and etched-TiO_2 electrodes, respectively, similar to that reported for the rutile TiO_2.[4,28] Then, the conduction band (CB) edge can be obtained according to the following equation,[24]

$$E_{CB} = E_{fb} + \kappa T \ln(N_C/N_D) \quad (1)$$

where N_C is the effective density of states with typical value of 10^{20} cm^{-3}. Other parameters have their usual meaning.

The band gap energy E_g was estimated from the plot of $(i_{ph} h\nu/\Phi_0)^{1/2}$ versus photon energy ($h\nu$), as shown in the inset of Figure 2. The intercept of the tangent to the plot gives a good approximation of band gap energy, which is about 3.15 and 3.04 eV for the unetched and etched TiO_2 films, respectively. These values are basically consistent with those estimated from the onset of light absorption of the films,[30] i.e., the intersection of the tangent at low and high frequency as shown in Figure 5, which corresponds to a wavelength of 395 and 401 nm or a band gap of 3.14 and 3.09 eV for the unetched and etched TiO_2 films, respectively. Band gap narrowing due to fluorination was also found for the F-doped TiO_2.[13] Once E_g is known, then the energy level of valence band edge E_{VB} can be easily obtained. It was found that after etching, the VB edge position was negatively shifted by ca. 0.23 V. The schematic energy level diagram for the electrode interface is presented in Scheme 1.

3.7. PC Activity. To evaluate the PC activities of the film electrodes, the photodegradation of the model pollutants in aqueous solutions at pH 3 was conducted in terms of photocatalysis (under open circuit) and photoelectrocatalysis (with an applied potential of +1 V). A plot of $\ln(C_0/C)$ versus irradiation time is presented in Figure 8. In all cases, the etched-TiO_2 displays a higher activity than the unetched for the photodegradation of three different pollutants under similar conditions.

3.8. Stability of Electrodes. It has been reported that TiO_xF_y ($x = 0-1$, $y = 1-4$) is unstable at ambient condition.[14] However, as suggested by the XPS results, it was found that

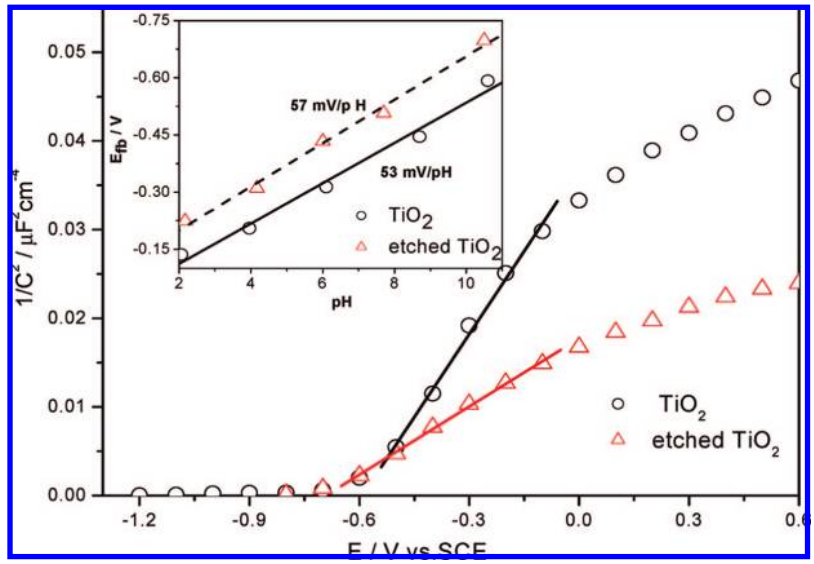

Figure 7. Mott–Schottky plots of the unetched and etched-TiO_2 electrodes in 0.5 M Na_2SO_4 at pH 10. Experiments were performed by applying the starting potential for 1 min and then performing a potential scan from positive to negative with a potential step of 50 mV and equilibrium time for 10 s at each potential. The frequency was 1 kHz. (Inset) pH dependence of the flat band potential obtained from the M-S plots, the line corresponding to a slope of 57 mV for the etched and 53 mV for pure TiO_2, respectively.

SCHEME 1: Schematic Energy Level Diagrams for the TiO_2 and the Etched-TiO_2, Estimated from the Flat Band Potential and the Band Gap Energy, with the Difference between the Bottom of the Conduction Band and Fermi Level Being Assumed to be about 0.15 V[a]

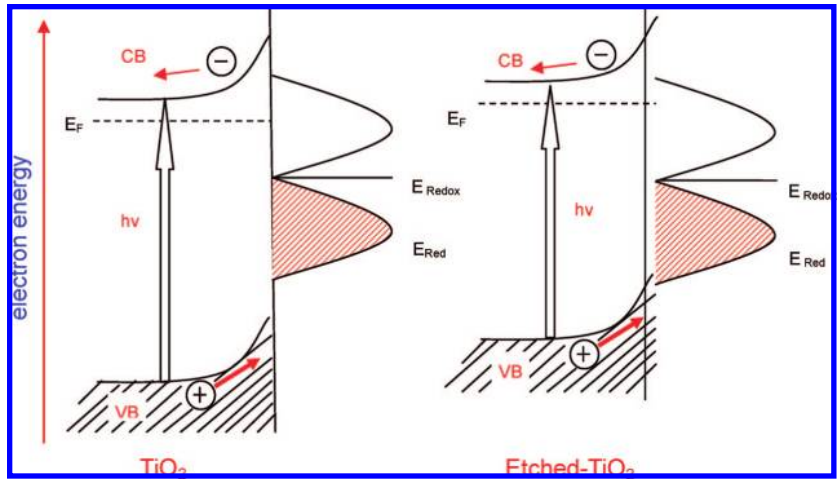

[a] VB = valence band, CB = conduction band. Other symbols have their usual meaning. For more details, see the text.

the etched TiO_2 electrode was stable even after having been used for 5 times for the PEC test. The photocurrent also remained almost unchanged. Repeat PC experiments for X3B photodegradation showed that the reaction rate was almost the same for the first and the fifth runs (Figure S3, Supporting Information). These results demonstrate that the F-containing TiO_2 electrode has an excellent stability against fluoride desorption under the present conditions.

4. Discussion

As stated above, high PC activity for the etched electrode was observed not only under open circuit but especially under a high bias potential where the contribution of photogenerated electrons to the degradation rate should be minor. This indicates efficient holes transfer to the solution either directly or indirectly via hydroxyl radicals occurring therein. In addition, an enhanced photooxidation rate was observed even for phenol which has been reported to be poorly adsorbed to the electrodes;[6,7] thus, its concentration on the surface of the electrodes can be regarded to be the same as that in the bulk solution. This at least indicates that the difference in PC activity between the two electrodes can not be attributed to different surface concentrations in this case. So, judging from the above results, just photogenerated holes are considered here to explain both the enhanced PEC and PC activities.

As a result of anodically etching of the TiO_2 in the HF solutions, two distinct effects can be found. The first is the change in the morphology of the surface; the second is the surface fluorination. In this paper, both effects will be discussed separately, and only in a qualitative way. Due to the complexity of the phenomena, a quantitative modeling is not possible at present.

4.1. Effects of Light Absorption on the Enhanced Activities. Textured windows that scatter the incident light are frequently used in solar cell devices for a more effective absorption of the light.[31] As a result of etching, the original

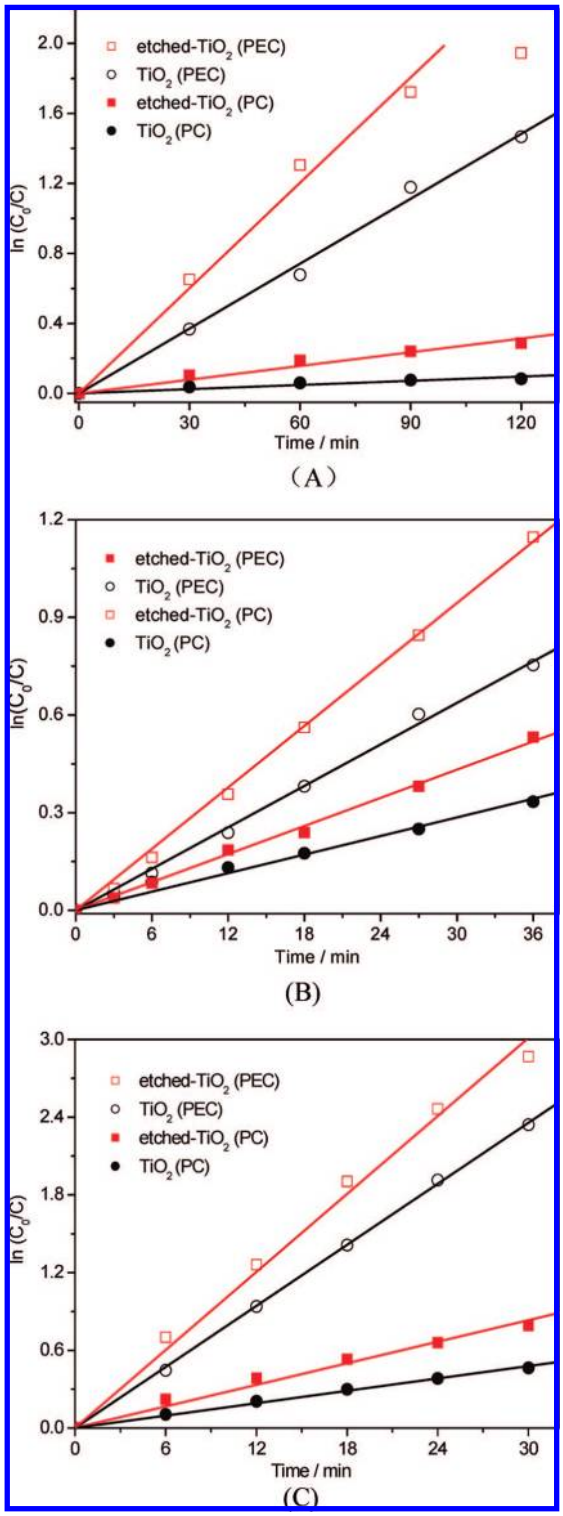

Figure 8. Photodegradation of (A) phenol, (B) MB, and (C) X3B on the etched and unetched TiO_2 film electrodes under open circuit (PC) and 1.0 V (PEC).

quite smooth surface became microrough. This may lead to a decrease of the reflectivity of the incident light, and/or more effective absorption of photons due to their scattering at the microrough surface. However, it is clear that the absorption spectra of the etched-TiO_2 showed a weaker intensity in UV–vis range compared with that of TiO_2 as indicated in Figure 5. Therefore, the enhanced activities can not be explained by a more effective absorption of photons (producing more electrons/holes).

4.2. Effects of the Morphology Obtained on the Enhanced Activities. The formation of porous structure due to etching must introduce a larger specific surface area, which is favorable for reactant adsorption. Thus, this increased adsorption should be an important reason for the enhancement of the photoreactivity. However, it is difficult to accurately measure the true surface area of the film. The surface area of the porous electrode could be evaluated by measuring the capacitance in the dark at a low band bending at which the inner edge of the depletion layer follows the contours of the porous structure.[32] From Figure 7 it is clear that the capacitance for a relatively small bending ($U = 0.0$ V) increases considerably after etching. For instance, at 0.0 V, the capacitance of the etched-TiO_2 (approximately 0.18 μF cm^{-2}) is larger than that of the TiO_2 (0.12 μF cm^{-2}). If the enhanced photoresponse totally resulted from the change in the surface area, the ratio of the photocurrent for the etched and unetched electrode should be 3:2. However, the actual ratio is more than 2 as calculated from Table 1. Furthermore, as can be seen in Figure 9, the photocurrent for the etched TiO_2 electrode was decreased markedly after the electrode was annealed at 400 °C in air, whereas it was kept unchanged for the unetched electrode heated at the same conditions. Note that such a sintering (lower than 600 °C at which the TiO_2 was prepared) did not change the morphology of the electrodes (Figure 3C and B1). Hence, the decrease in the photocurrent in this case should be irrelevant to surface morphology. In other words, these results further indicate that the enhanced activities cannot be explained by the increase in surface area alone. In fact, it was found from Figure 4A that fluorine concentration on the surface of the etched electrode after heating was dramatically reduced, similar to the result that the concentration of fluoride on the surface of freshly prepared TiO_2 nanotubes by anodic oxidation of titanium was nearly lost in the following annealing process.[21] From these results, so we can infer that the surface fluorination due to etching should also contribute to the enhanced photoactivities of the TiO_2. This will be further discussed in the next section.

4.3. Mechanism of Surface Fluorination on Enhanced Activities. To account for the increase in photoactivity due to such a fluorination, explanations have been proposed from different perspectives. For instance, it was argued that the fluorination influenced the surface acidity and thus increased the adsorption of target pollutants on the surface of TiO_2.[16] But this can not explain the fact that the increase can still be observed even when the absorption of pollutants is inhibited on the surface of fluorinated-TiO_2. In this work, the fluorination is different to some extent from those that happened in solutions containing F^- ions. It is not a simple replacement of hydroxyl groups or oxygen atoms by fluoride as indicated by XPS results. In addition, this surface fluorination is relative stable. It is more like a kind of surface fluoride doping. Both changes may influence the photoreactivity at least via the following manners.

First, the presence of surface states at the interface is commonly believed to be important in dictating the charge-transfer process.[33,34] Occupied surface states can usually act as the recombination centers of photogenerated minority carriers, and thus, their presence is usually unfavorable to the photoreactivity of material. Grätzel et al.[34] have pointed out that as the water coordinated to Ti (IV) was replaced by the adsorbates, the trap depth of the surface state was expected to decrease, and if the Lewis basicity of the ligand was strong enough, the electronic level of the surface state would be swept into the conduction band implying that its trapping action would vanish, suggesting the removal of surface states by complexation with

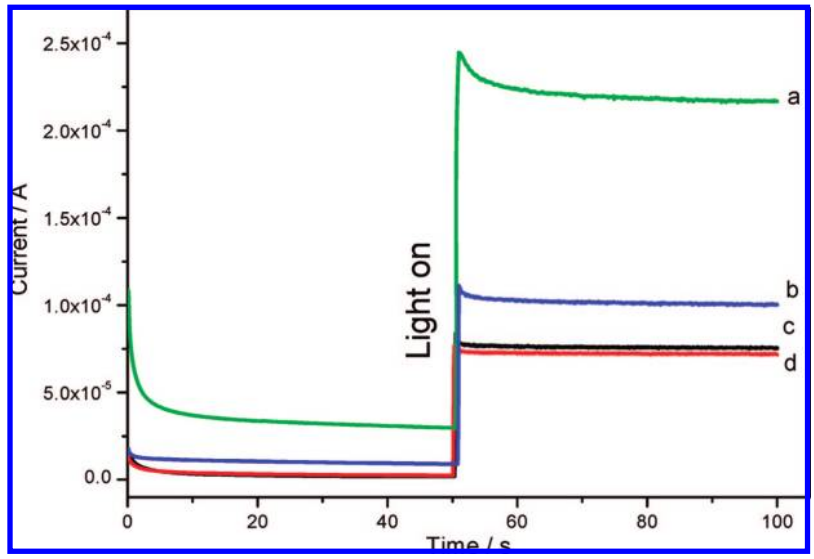

Figure 9. Time dependence of current in pH 3 blank electrolyte at +0.8 V in the dark and under illumination for (a) the etched-TiO_2 electrode, (b) same to (a) but then annealed at 400 °C for 2 h, (c) the TiO_2 electrode, (d) same to (c) but then annealed at 400 °C for 2 h.

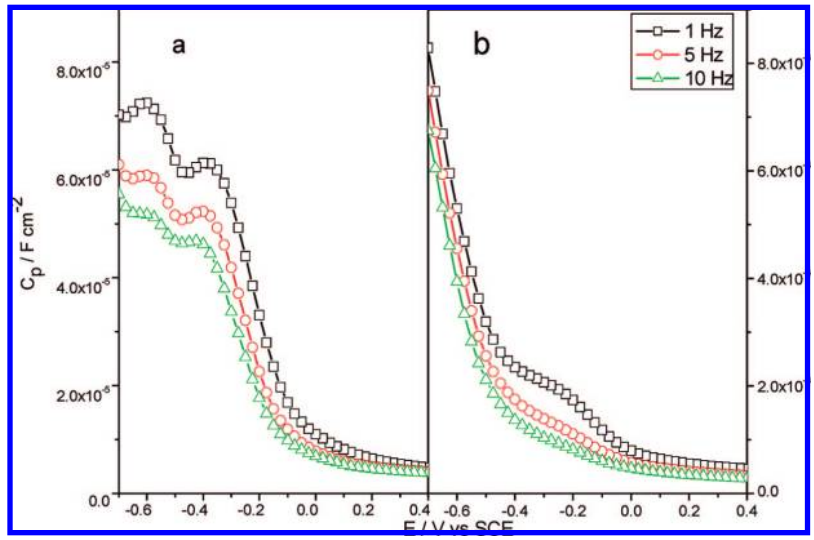

Figure 10. Measured parallel capacitance (C_p) versus the applied potential plot at various frequencies in 0.5 M Na_2SO_4 solutions (pH 3) in the dark for (a) TiO_2 and (b) etched-TiO_2. These experiments were performed by stepping the potential from positive to negative potential, and the EIS response was measured at each potential.

the adsorbates. Fluoride ions with the ability to specific adsorption on TiO_2, may act as a kind of lewis base. So we speculate that the fluoride on the surface might decrease surface state density and even possibly give rise to new surface states. This can be demonstrated by impedance analysis as indicated below. Analyses of the impedance due to surface states in the dark were conducted by using the approach reported by Searson et al.[35] and us.[36] This provides a convenient method for distinguishing between the various interface states.[35] Figure 10 shows the parallel capacitance (C_p) under various conditions plotted against the applied potential in the dark. As shown in Figure 10a, there are two peaks that appeared at frequencies lower than 10 Hz for the TiO_2 located at about −0.6 and −0.4 V. According to the previous conclusion, the different positions of the capacitance peak may involve diverse surface states. This indicates that there are two kinds of surface states on the TiO_2 electrode, whereas for the etched-TiO_2, the two peaks vanish and a new peak at −0.2 V emergences at lower frequencies as shown in Figure 10b. These indicate that the etching quenched or decreased the original surface states of the TiO_2 and even possibly gave rise to new surface states. Note that the magnitude of C_p of the etched-TiO_2 is higher than that of the TiO_2 should result from its large surface area. The decrease in the density of surface states is also supported by the results of PL as discussed above. The possibly produced new surface states and/or the shift in the positions of surface states do not give any signal in the PL spectr, may be due to them acting as nonradiative recombination sites.

Second, in most cases of doping[23] or surface modification,[14] the energy band structure of the semiconductor material, containing the flatband potential and midgap energy level, could change, which is commonly believed to be important in dictating the charge-transfer process on the surface. According to the Marcus theory, the electron tunneling process must take place between states of equal energy.[33,37,38] For the TiO_2/aqueous system, because the equilibrium level of the redox couple in solution is located considerably above the top of the valence band at the surface, the probability of direct hole transfer to the solution should be very low (shown in Scheme 1). Whereas for the etched-TiO_2 system, because the energy band shifted negatively, the energetic overlap between the valence band edge at the surface and the filled levels of the redox couple in the

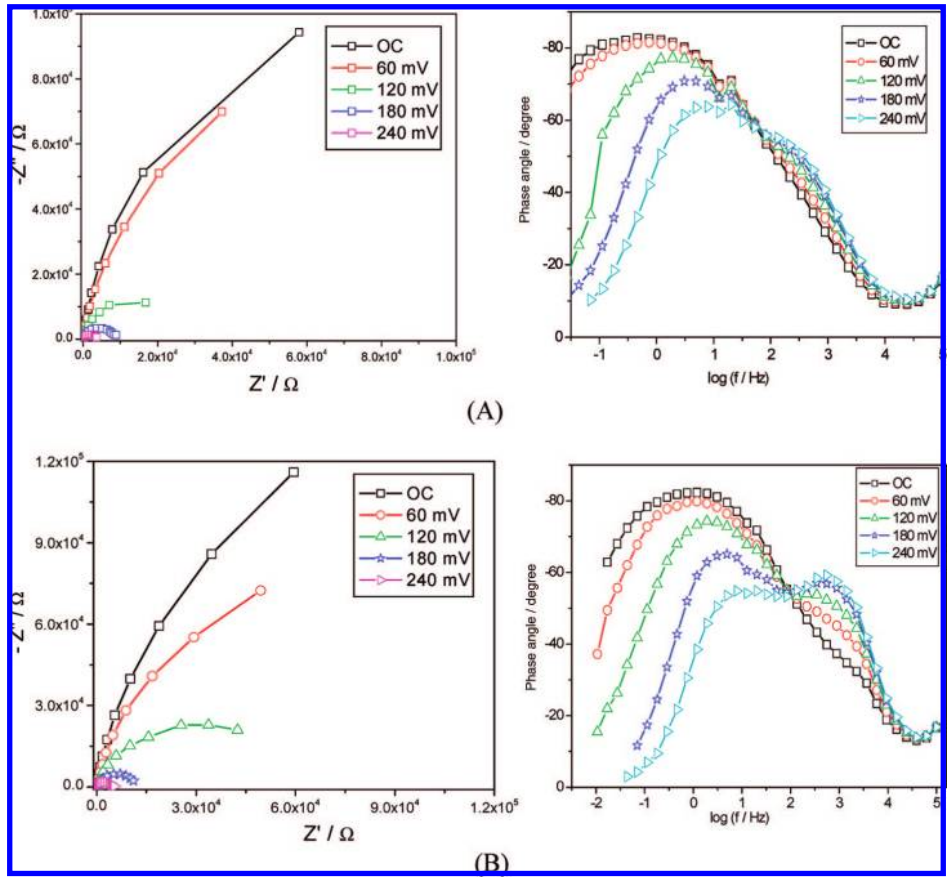

Figure 11. EIS response of (A) etched-TiO_2 and (B) TiO_2 under different bias potentials versus open circuit (OC) in 0.5 M Na_2SO_4 solutions (pH 3) with illumination.

solution was increased, the probability of direct holes transfer to the solution should increase, thereby increasing the photocurrent.

Electrochemical impedance spectroscopy (EIS) also provides a powerful method for the study of charge transfer and recombined processes at the semiconductor/electrolyte interfaces.[36,39–41] A typical EIS plot obtained at different potentials in blank Na_2SO_4 aqueous solutions (pH 3) for the illuminated TiO_2 and etched-TiO_2 is shown in Figure 11. In our previous report,[36] it was found that electrode potential was the only state variable in this case, making analysis of such a process relative simple. First, the resistance R_S resulting from the solution, contacts, and the leads can be estimated from the real part of the EIS at very high frequencies. The same R_S of about 10 Ω for the two electrodes was observed, which indicates that the conductivity of the films did not change. Thus, the enhanced activities can not be attributed to this. Second, as shown in the Nynquist plots, after etching, the visible EIS arc of the electrode becomes smaller at the same potential. According to previous results,[36,41] the smaller size of the semicircle arc diameter indicates a more effective separation of photogenerated electron–hole pair and/or a faster interfacial charge transfer to the electron donor/acceptor. Note that the two peaks on the Bode plot are more evident for the pure TiO_2. We have ever proposed that the first peak at relative high-frequency is attributed to the combined space charge/surface state/oxide film capacitances and associated resistances.[36] However, in the case of the etched-TiO_2, the first peak in the Bode plot at high-frequency becomes indistinguishable, which should be attributed to the change of surface state capacitance as revealed by the C_p experiments. From these results, it infers that the enhanced activities result from the more efficient interface reactions.

In summary, it follows that the surface fluorination in the experiments resulted not merely in a reduction of the rate of surface recombination but in virtual enhancement of the process of charge transfer.

5. Conclusions

Surface-fluorinated TiO_2 nanoporous film can be prepared by anodically etching of TiO_2 in HF-containing solutions. Highly enhanced PEC performance and PC activities for the degradation of target pollutants, phenol, methylene blue, and X3B on the etched-TiO_2 were observed. The improvements can be attributed to the enhanced surface area, negative-shifted appearing energy band edges, decreased surface recombination centers, and/or favorable charge transfer rate. The results presented in this work indicate a strategy of electrochemically immobilizing fluorine for improving the photoreactivity of junctions of polycrystalline TiO_2/aqueous and are potentially useful in a number of applications including photocatalysis and chemical conversion of solar energy by splitting of water.

Acknowledgment. This project was supported by the National Science Foundation Council of China (NSFC, Grant Nos. 20373062 and 20107006) and Zhejiang Applied Chemistry priority disciplines open fund (07/01/2006).

Supporting Information Available: I−E relationship of the anatase TiO_2 electrode (Figure S1), XRD patterns and Raman spectra of the etched and unetched rutitle TiO_2 electrode (Figure S2), and the stability of the etched TiO_2 (Figure S3). This material is available free of charge via the Internet at http://pubs.acs.org.

References and Notes

(1) Hagfeldt, A.; Grätzel, M. *Chem. Rev.* **1995**, *95*, 49.
(2) Hoffmann, M. R.; Martin, S. T.; Choi, W.; Bahnemann, D. W. *Chem. Rev.* **1995**, *95*, 69.
(3) Linsebigler, A. L.; Lu, G.; Yates, T. J. *Chem. Rev.* **1995**, *95*, 735.
(4) Kavan, L.; Grätzel, M.; Gilbert, S. E.; Klemenz, C.; Scheel, H. J. *J. Am. Chem. Soc.* **1996**, *118*, 6716.
(5) (a) Leng, W. H.; Liu, H.; Cheng, S. A.; Zhang, J. Q.; Cao, C. N. *J. Photochem. Photobiol. A* **2000**, *131*, 125. (b) Leng, W. H.; Zhang, Z.; Zhang, J. Q. *J. Mol. Catal. A: Chem.* **2003**, *206*, 239. (c) Leng, W. H.; Zhu, W. C.; Ni, J.; Zhang, Z.; Zhang, J. Q.; Cao, C. N. *Appl. Catal., A* **2006**, *300*, 24.
(6) (a) Minero, C.; Mariella, G.; Maurino, V.; Pelizzetti, E. *Langmuir* **2000**, *16*, 2632. (b) Minero, C.; Mariella, G.; Maurino, V.; Vione, D.; Pelizzetti, E. *Langmuir* **2000**, *16*, 8964.
(7) (a) Park, H.; Choi, W. *J. Phys. Chem. B* **2004**, *108*, 4806. (b) Choi, W. *Langmuir* **2004**, *20*, 11523.
(8) Park, H.; Choi, W. *Catal. Today* **2005**, *101*, 291.
(9) Lv, K.; Xu, Y. *J. Phys. Chem. B* **2006**, *110*, 6204.
(10) Maurino, V.; Minero, C.; Mariella, G.; Pelizzetti, E. *Chem. Commun.* **2005**, 2627.
(11) (a) Mrowetz, M.; Selli, E. *Phys. Chem. Chem. Phys.* **2005**, *7*, 1100. (b) Mrowetz, M.; Selli, E. *New J. Chem.* **2006**, *30*, 108.
(12) Hattori, A.; Shimoda, K.; Tada, H.; Ito, S. *Langmuir* **1999**, *15*, 5422.
(13) Yu, J. C.; Yu, J.; Ho, W.; Jiang, Z.; Zhang, L. *Chem. Mater.* **2002**, *14*, 3808.
(14) (a) Wang, C. M.; Mallouk, T. E. *J. Phys. Chem.* **1990**, *94*, 423. (b) Wang, C. M.; Mallouk, T. E. *J. Phys. Chem.* **1990**, *94*, 4276.
(15) Subbarao, S. N.; Yun, Y. H.; Kershaw, R.; Dwight, K.; Wold, A. *Inorg. Chem.* **1979**, *18*, 488.
(16) Tang, J.; Quan, H.; Ye, J. *Chem. Mater.* **2007**, *19*, 116.
(17) Li, D.; Haneda, H.; Hishita, S.; Ohashi, N.; Labhsetwar, N. K. *J. Fluorine Chem.* **2005**, *126*, 69.
(18) Li, D.; Haneda, H.; Hishita, S.; Ohashi, N. *Chem. Mater.* **2005**, *17*, 2596.
(19) (a) John, C. F.; Melissa, M. R.; Gerard, M. S.; Paul, A. K. *J. Electrochem. Soc.* **1999**, *146*, 1960. (b) Peter, M. H.; Inge, E. V.; Peter, C. S. *J. Electrochem. Soc.* **2000**, *147*, 2999. (c) Solanki, C. S.; Bilyalov, R. R.; Poortmans, J.; Celis, J. P.; Nijs, J.; Mertens, R. *J. Electrochem. Soc.* **2004**, *151*, C307.
(20) (a) Nakato, Y.; Akanuma, H.; Shimizu, J-I.; Magari, Y. *J. Electroanal. Chem.* **1995**, *396*, 35. (b) TsujikoA.; Kisumi, T.; Magari, Y.; Murakoshi, K.; NakatoY., *J. Phys. Chem. B* **2000**, *104*, 4873.
(21) Ruan, C.; Paulose, M.; Varghese, O. K.; Mor, G. K.; Grimes, C. A. *J. Phys. Chem. B* **2005**, *109*, 15754.
(22) Masuda, H.; Kanezawa, K.; Nakao, M.; Yokoo, A.; Tamamura, T.; Sugiura, T.; Minoura, H.; Nishio, K. *Adv. Mater.* **2003**, *15*, 159.
(23) Shi, J. Y.; Leng, W. H.; Zhu, W. C.; Zhang, J. Q.; Cao, C. N. *Chem. Eng. Technol.* **2006**, *29*, 146.
(24) Cheng, X. F.; Leng, W. H.; Liu, D. P.; Zhang, J. Q.; Cao, C. N. *Chemosphere* **2007**, *68*, 1976.
(25) Jing, L.; Xin, B.; Yuan, F.; Xue, L.; Wang, B.; Fu, H. *J. Phys. Chem. B* **2006**, *110*, 17860.
(26) Baiju, K. V.; Shukla, S.; Sandhya, K. S.; James, J.; Warrier, K. G. K. *J. Phys. Chem. C* **2007**, *111*, 7612.
(27) Yoon, M.; Seo, M.; Jeong, C.; Jang, J. H.; Jeon, K. S. *Chem. Mater.* **2005**, *17*, 6069.
(28) Cooper, G.; Turner, J. A.; Nozik, A. J. *J. Electrochem. Soc.* **1982**, *129*, 1973.
(29) Yasumichi, M.; Toru, Y.; Ei-ichi, S. *J. Electrochem. Soc.* **1989**, *136*, 1389.
(30) Kontos, A. I.; Arabatzis, I. M.; Tsoukleris, D. S.; Kontos, A. G.; Bernard, M. C.; Petrakis, D. E.; Falaras, P. *Catal. Today* **2005**, *101*, 275.
(31) Soltz, D.; Cescato, L.; Decker, F. *Solar Energy Mater. Solar Cells* **1992**, *25*, 179.
(32) Lagemaat, J. V. D.; Plakman, M.; Vanmaekelbergh, D.; Kelly, J. J. *Appl. Phys. Lett.* **1996**, *69*, 2246.
(33) Masahiko, N. *J. Appl. Phys.* **1980**, *51*, 1669.
(34) Moser, J.; Punchihewa, S.; Infelta, P. P.; Grätzel, M. *Langmuir* **1991**, *7*, 3012.
(35) (a) Oskam, G.; Schmidt, J. C.; Hoffmann, P. M.; Searson, P. C. *J. Electrochem. Soc.* **1996**, *143*, 2531. (b) Oskam, G.; Schmidt, J. C.; Searson, P. C. *J. Electrochem. Soc.* **1996**, *143*, 2538.
(36) Leng, W. H.; Zhang, Z.; Zhang, J. Q.; Cao, C. N. *J. Phys. Chem. B* **2005**, *109*, 15008.
(37) Nozik, A. J.; Memming, R. *J. Phys. Chem.* **1996**, *100*, 13061.
(38) Peter, L. M. *Chem. Rev.* **1990**, *90*, 753.
(39) Bisquert, J.; Garcia-Belmonte, G.; Fabregat-Santiago, F.; Ferriols, N. S.; Bogdanoff, P.; Pereira, E. C. *J. Phys. Chem. B* **2000**, *104*, 2287.
(40) (a) Li, H.; Cheng, S. A.; Wu, M.; Wu, H. J.; Zhang, J. Q.; Li, W. Z.; Cao, C. N. *J. Phys. Chem. A* **2000**, *104*, 7016. (b) Liu, H.; Li, X. Z.; Leng, Y. J.; Li, W. Z. *J. Phys. Chem. B* **2003**, *107*, 8988.
(41) Leng, W. H.; Zhang, Z.; Cheng, S. A.; Zhang, J. Q.; Cao, C. N. *Chin. Chem. Lett.* **2001**, *12*, 1019.

JP7097476